# Halogen-Bond-Based Organocatalysis Unveiled: Computational Design and Mechanistic Insights

Nika Melnyk,[†] Rica Garcia,[†] and Cristina Trujillo[*,‡,†]

†*Trinity Biomedical Sciences Institute, School of Chemistry, The University of Dublin, Trinity College, D02 R590 Dublin 2, Ireland*

‡*Department of Chemistry, University of Manchester, Oxford Road, Manchester M139PL*

E-mail: cristina.trujillodelvalle@manchester.ac.uk

**Abstract**

Halogen-bond-based organocatalysis is a promising alternative to the extensively explored halogen-bond-based catalysis. This paper presents a comprehensive theoretical investigation of the structural and electronic properties of the $\sigma$-hole, as well as the computational design of a series of electronically activated monodentate and bidentate iodine and benzimidazolium achiral donor systems, inspired by experimental and computational papers published in the last decade. The aforementioned activation modes are compared, and the mechanistic details of the reaction are discussed.

## Introduction

Halogens, being relatively electronegative elements, exhibit exceptional nucleophilic properties in their anionic state.[1] However, this nucleophilicity diminishes as they transition into a diatomic state through the formation of covalent bonds with more electronegative atoms. Consequently, this leads to the emergence of an electron-deficient or electrophilic region

known as a $\sigma$-hole.[2–7] Experimental evidence of this phenomenon was reported as early as 1819[8] by Pelletier and Caventou when they found attractive interactions between dihalogens and anions. However, it was theoretical studies conducted by Politzer and Murray in the 1990s[9,10] which provided explicit insights into the origin and electronic properties of the $\sigma$-hole, ultimately describing the entity as the result of an anisotropic charge distribution on the surface of a covalently bound halogen atom. These theoretical findings sparked curiosity and laid a foundation for further research carried out in the early 2000s, confirming the findings of Politzer and Murray.[11,12] The interest surrounding the $\sigma$-hole culminated in an initiative led by the International Union for Pure and Applied Chemistry (IUPAC) aimed at taking a comprehensive look at intermolecular interactions involving halogens as electrophilic species.[13,14] The project concluded in 2013, ultimately defining a halogen-bond (XB) interaction as a net attractive interaction between an electrophilic region associated with a halogen atom in a molecular entity and a nucleophilic region in another, or the same molecular entity.[15,16] While the $\sigma$-hole model has been widely employed to explain the strength of XB, recent studies reveal that other components, such as electrostatics, charge transfer (CT), polarisation, and dispersion, play crucial roles in providing a complete understanding of these interactions.[17–19] In 2021, the existence of the $\sigma$-hole was experimentally demonstrated using Kelvin probe force microscopy,[20] providing tangible evidence for a theory that has been postulated for more than a century. This cutting-edge technique allowed the direct imaging of the asymmetric electronic charge distribution and the shape of the $\sigma$-hole in a brominated molecule, marking a significant milestone in the field of $\sigma$-hole interactions.

In fact, the XB has emerged as a versatile tool with applications in a wide range of domains. In particular, it has been used extensively in fields such as crystal engineering,[4] supra-molecular chemistry,[4] drug design[21] and bio-molecular engineering.[22] These applications have propelled the XB to the forefront of modern chemistry and materials science, promising exciting future prospects. In more recent developments, the XB has ventured into the domain of non-covalent organocatalytic applications, drawing inspiration from the

undeniable success of hydrogen-bond (HB)-based organocatalysis.[23–32] While both the HB and XB share advantageous features such as their electrophilic nature,[4] it is the distinctive properties of XB donor systems[33,34] that emphasise their potential as a promising alternative to the extensively investigated HB-based catalysis. In comparison to the latter, the XB offers a higher level of tunability.[4,15] The strength of the XB interaction can be adjusted by modifying the electron-withdrawing characteristics of the covalently bound scaffolding to the halogen atom as well as the polarisability of the XB-donor atom. The size of the $\sigma$-hole, which determines the directionality of the XB-donor system (see Figure 1), is directly proportional to the polarisability of the XB-donor atom.[35] This directionality arises from the repulsive forces between the perpendicular lone pairs of electrons, known as the electron belt, and the $\sigma$-hole.[36,37] Recently, Keuper *et al*[38] leveraged the directional nature of an XB-donor to devise a novel and highly effective enantioselective organocatalytic strategy, demonstrated in the Reissert-type anion-binding reaction. Furthermore, the XB donor exhibits distinctly larger van der Waals radii and hydrophobicity compared with the HB donor counterpart, making it more soluble in non-polar solvents and sensitive to steric hindrance.[4] Consequently, the XB donor is less prone to competition with more polar solvents, which accounts for the applicability of the XB donor in a wide range of organic reactions.

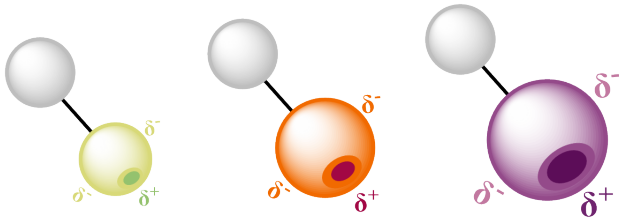


Figure 1: Origin of XB directionality illustrated in different XB-donors of increasing polarisability namely chlorine (green), bromine (orange) and iodine (purple).

Although the implication of XB-donor moieties within organocatalysis is in its infancy, its progression is certainly noteworthy, as there has been a substantial amount of neutral and cationic XB-donor organocatalysts developed since its initial reporting in 2008 when C. Bölm *et al*[39] demonstrated the reduction catalysed by haloperfluoroalkane of 2-phenylquinoline by

the Hantzsch ester. However, it is essential to acknowledge that the majority of XB-based organocatalytic examples reported in the literature are achiral. A recent literature review conducted by Peluso *et al*[40] focused on enantioselective XB-based organocatalysis over the last decade draws attention to the limited and underdeveloped applications of the XB-bond donor as the primary contributor to selectivity.

In this paper, we present a comprehensive theoretical analysis of a diverse range of electronically activated monodentate and bidentate achiral XB-donor catalysts, inspired by experimental and computational studies published in the last decade (see Scheme 1). Despite the considerable research dedicated to XB-based catalysis during this decade, the nature of the XB-interaction remains a subject of debate. To advance the field towards asymmetric applications, it is imperative to effectively characterise the XB-interaction upon complexation with nucleophilic substrates. This study takes into account various critical factors such as the XB-donor atom, substrate binding mode, and the electronic and steric characteristics of the catalytic scaffolding. By thorough exploration of these factors, our study aims to shed light on the intricacies of XB-based catalysis and contribute to the development of more efficient and selective catalysts.

In 2011, Huber *et al*[41] demonstrated the efficiency of achiral cationic and neutral XB-based organocatalysts in activating benzhydryl bromide through halide abstraction. Furthermore, in recent years, Gliese *et al*[42] experimentally evaluated a series of monodentate and bidentate achiral XB-based organocatalysts in the C-C coupling step of Michael addition of indole to *trans*-crotonophenone. This series of achiral XB-based organocatalysts presented in the aforementioned experimental studies exhibited a wide range of variations in the catalytic scaffolding, including the XB-donor atom and substituents. The diverse structural characteristics observed in these experimental studies motivated us to conduct a comprehensive theoretical investigation of the structural and electronic properties of the $\sigma$-hole. Furthermore, we aimed to computationally design new achiral bidentate XB-based organocatalysts. In 2023, an intriguing study published by Raphaël *et al*[43] theoretically

compared the widely accepted O-activation mode and the overlooked direct $\pi$-type activation mode of XB-donor organocatalysts in reactions involving $\alpha,\beta$-unsaturated carbonyl compounds. This study provided insight into alternative mechanisms of XB-based catalysis, which inspired us to investigate and compare these activation modes in a series of organocatalysts based on achiral iodine, including structurally simple yet robust molecular iodine,[44] in the context of the Michael addition of indole to *trans*-crotonophenone. Our study aims to clarify the importance of considering multiple factors in the design of novel XB-based organocatalysts. These factors include the electronic properties of substituents, CT, steric hindrance, catalytic deformation energy, and activation modes. By comprehensively exploring these elements, we aim to provide a deeper understanding of XB-based catalysis and contribute to the design of efficient and selective XB-based organocatalysts.

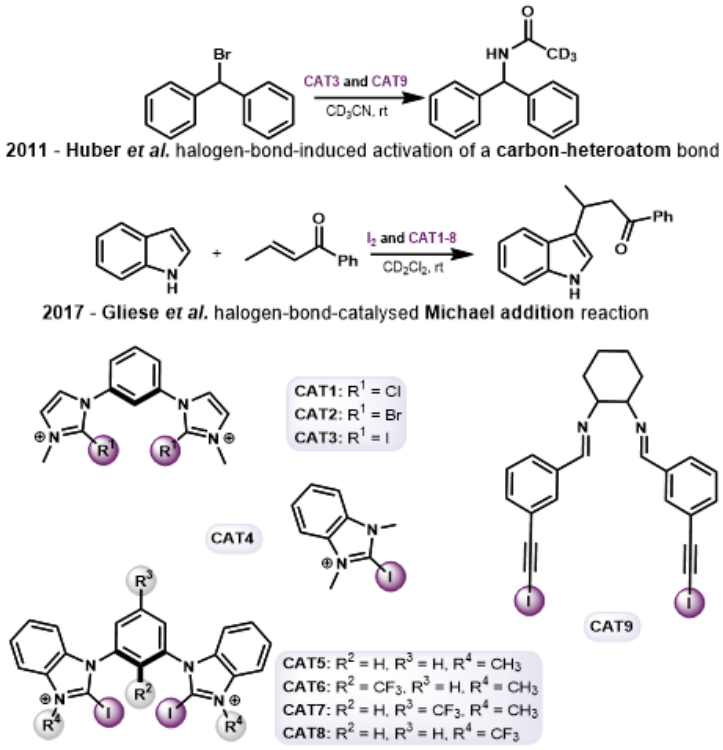


Scheme 1: Organic reactions and XB-based organocatalysts evaluated and discussed in this work.

# Computational details

Structures of the complexes and monomers under study were optimised using the Gaussian09 package[45] at the computational level ωb97xd/def2-svp, in addition, pseudopotentials were incorporated for iodine-based systems. Solvent effects, using dichloromethane (DCM) as the solvent for the Michael addition reaction and acetonitrile (ACN) for the halide abstraction reaction, were included in the optimisation by means of the solvation model based on the density approach (SMD) implemented in Gaussian09.[45] Single point energies for lowest energy small basis set calculations were computed using ωb97xd/def2-tzvp. The molecular electrostatic potentials (MEPs) for all catalytic systems were computed using the Gaussian09 software,[45] employing 0.001 a.u. isosurfaces of the electron density.[46] The molecular electrostatic potential (MEP) results obtained were further analysed and quantified using Multiwfn[47] and plotted using Jmol. To evaluate the electron density of the different systems under study, Atoms in Molecules (AIM) methodology[46] was used, using the AIMAll program.[48] The natural bond orbital (NBO) was employed to evaluate atomic charges using the NBO-7 program.[49]

Furthermore, an energy decomposition analysis based on the Localized Molecular Orbital Energy Decomposition Analysis (LMO-EDA) scheme[50] was performed. The LMO-EDA approach allows for a detailed investigation of the energetic contributions of different components in the systems studied. The analysis was carried out at the computational level m06-2x/def2-svp in the gas phase with the inclusion of pseudopotentials. The GAMESS program (version 2018-R2) was used for the calculations, and the structures used for this study were re-optimised in the specified computational details.[51]

# Results and discussion

## Halide abstraction

### Energetic analysis

We conducted an in-depth investigation into the characteristics of the halide abstraction reaction facilitated by XB-based organocatalysts CAT3 and CAT9 (Scheme 1). These catalysts have been subject to previous experimental testing,[41,52] where their catalytic activities were reported to be quite similar under equivalent experimental conditions. However, the literature lacks explicit details on the binding mode and mechanistic pathways involved.

Our primary objective was to shed light on this chemical transformation and to offer valuable mechanistic insights by investigating the catalytic role of XB-donor systems. In doing so, we aimed to gain a comprehensive understanding of the halide abstraction reaction. The literature presented two possible mechanistic pathways, Pathway 1 and Pathway 2,[41,52] each providing a different perspective on how XB-donors interact with the R-Br leaving group. As illustrated in Figure 2, Pathway 1 proposed that the XB-donor interacts directly with the R-Br moiety, thereby facilitating the heterolytic bond cleavage of the R-Br bond. Alternatively, Pathway 2 suggested that the XB-donor interacts with the bromide anion generated from the uncatalysed heterolytic bond cleavage of the R-Br bond (Figure 2).

From a mechanistic perspective, the halide abstraction reaction, facilitated by both CAT3 and CAT9 catalysts, clearly manifested an energetic preference towards Pathway 1 (see Figure 2). This preference is evident as computational assessments for pathway 2 were unattainable. This indicates the reaction proceeds via a stepwise mechanism, wherein the XB donor activates the R-Br bond of the leaving group through XB-bonding (TS1). This activation process facilitates the heterolytic cleavage of the R-Br bond, leading to the formation of a carbocation intermediate (INT). Subsequently, in TS2, an acetonitrile molecule attacks the aforementioned carbocation intermediate, resulting in the formation of the final product (PROD). Consistent with experimental data found in literature,[41,52] the energetics of Path-

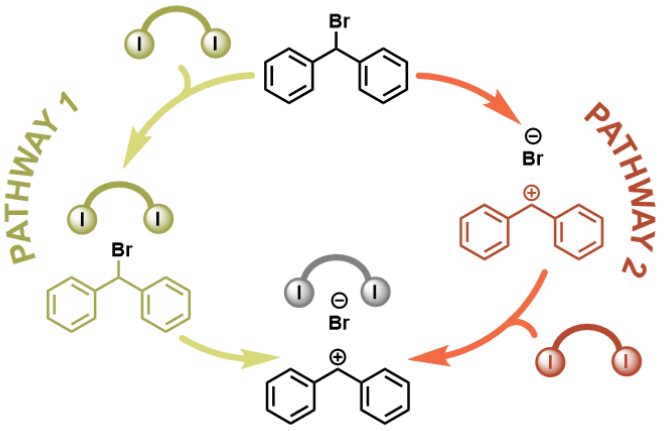


Figure 2: Mechanisms proposed by literature for the halide abstraction under the catalysed of XB-based catalysts; pathway 1 (yellow) and pathway 2 (orange).

way 1 under the catalysis of CAT3 and CAT9 were remarkably similar (Figure S1 and Table S1). Despite both catalytic systems having the potential to bind in a bidentate manner, CAT9 displayed a preference for the monodentate binding mode (Figure 3). This preference can be attributed to the tendency of the iodine atoms in CAT9 to orientate in opposite directions, as a result of geometric constraints (Figure S2 and S5)).

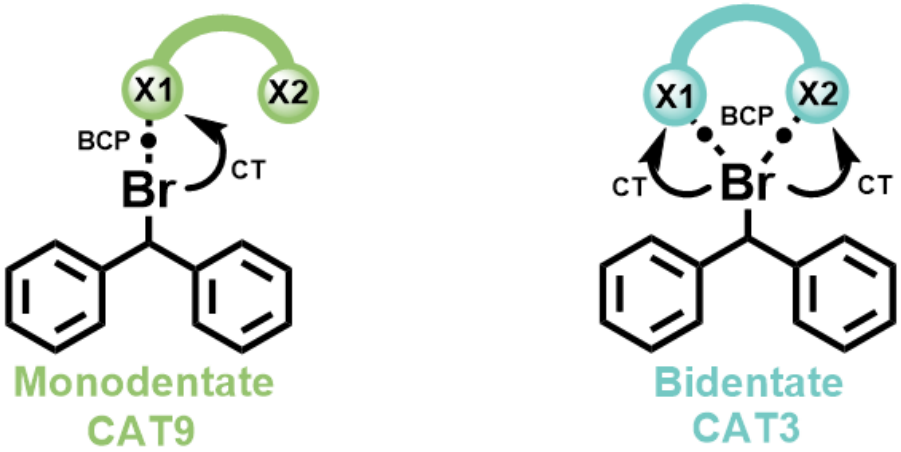


Figure 3: Monodentate (green) and bidentate (blue) binding modes found for CAT9 and CAT3 respectively.

## Quantification of the NCI

To quantify and validate the presence of non-covalent interactions (NCIs) within Pathway 1 of the halide abstraction reaction catalysed by XB-donors CAT3 and CAT9, computational methods QTAIM and NBO were employed. The key parameters of interest were the electron density at the critical bond point ($\rho_{BCP}$) and the CT, associated with the substrate-catalyst stabilisation interaction, as illustrated in Figure 3. Table 1 highlights the $\rho_{BCP}$ for the Br···I interaction within the CAT3 and CAT9 catalysed reaction pathway 1, which generally indicates a consistent noncovalent nature, representative of halogen bonding between the catalyst and substrate. The characterisation of CT upon complexation from the lone pair of electrons LP (Br) of the substrate and the non-bonding orbital of the catalyst BD* (C-I) was in agreement with the aforementioned QTAIM analysis (Table 2).

Table 1: $\rho$(BCP) (a.u.) of the Br···I interaction in Pathway 1 of the CAT3 and CAT9 catalysed halide abstraction.

| **CATALYST** | **$\rho$(BCP) (a.u.)** | **TS1** | **INT** | **TS2** | **PROD** |
|---|---|---|---|---|---|
| CAT3 | Br···X1 | 0.020 | 0.022 | 0.023 | 0.022 |
| | Br···X2 | 0.017 | 0.021 | 0.022 | 0.022 |
| CAT9 | Br···X1 | 0.024 | 0.023 | 0.023 | 0.023 |

Table 2: NBO E(2) (kcal/mol) of the Br···I interaction in pathway 1 of the CAT3 and CAT9 catalysed halide abstraction.

| **CATALYST** | **NBO E(2) (kcal/mol)** | **TS1** | **INT** | **TS2** | **PROD** |
|---|---|---|---|---|---|
| CAT3 | Br···X1 | 76.94 | 104.89 | 97.49 | 94.64 |
| | Br···X2 | 58.74 | 89.34 | 98.66 | 93.51 |
| CAT9 | Br···X1 | 86.48 | 98.70 | 99.45 | 102.97 |

Based on the similar catalytic activity reported for the halide abstraction reaction under the catalysis of both CAT3 and CAT9,[41,52] the data of $\rho_{BCP}$ and E(2) implies that the monodentate XB substrate stabilisation interaction, as seen for CAT9, is equivalent in efficiency to the bidentate XB interaction via CAT3. Despite the contrasting binding modes of these two catalytic systems, their catalytic performance appears to be comparable, indicating that

depending on the specific catalytic scaffolding, both the monodentate and bidentate binding modes can effectively facilitate the halide abstraction.

Further evaluation of the secondary interactions by the QTAIM method provided valuable insights regarding the underlying factors which dictate the binding modes preference of the XB-catalysed TS1 of the halide abstraction reaction. The presence of non-covalent secondary interactions acts as anchor points, enhancing the interactions between the substrate and the catalyst. In the case of the CAT9 catalysed reaction, these interactions were identified between the phenyl ring of the substrate and the phenyl rings of the catalyst (see Tables S6-S9 and Figure S5). These specific interactions play a critical role in facilitating and stabilising the unexpected monodentate binding mode of the CAT9 catalyst.

## Michael addition of indole to *trans*-crotonophenone

### Energetic analysis

To establish a solid basis for investigating a series of XB-based organocatalytic scaffolds, we conducted a comprehensive analysis of the electronic properties of a diverse range of monodentate and bidentate XB-donors ($I_2$ and CAT1-8, Scheme 1). In accordance with the $\sigma$-hole theory[14] the electronic properties of catalysts were investigated through MEP calculations. First, we compared the relative $V_{max}$ of the MEP in a series of bidentate XB-donor catalysts, exhibiting different XB-donor atoms, as illustrated in Figure 4 (CAT1-3).

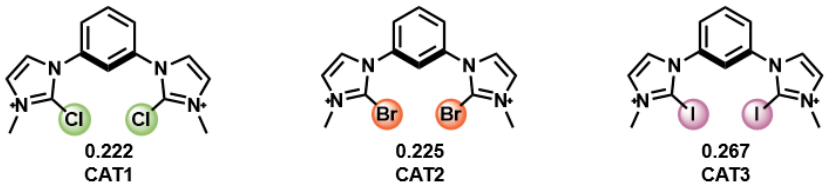


Figure 4: MEP on the 0.001 a.u. electron density isosurface and maxima ($V_{max}$) values in a.u. for the catalysts under study (CAT1-3).

As anticipated, the size of the $\sigma$-hole was in direct correlation with the polarisability of the XB-donor atom. The iodine atom being the most polarisable of all assessed XB donor

atoms, possessed the highest $V_{max}$ and thus the largest $\sigma$-hole (see supporting information Figure S8-S10). Subsequently, an in-depth examination of the effect of the substituent on the $\sigma$ hole was performed, maintaining a constant XB-donor atom while varying the catalytic scaffolding. The investigation focused primarily on evaluating factors such as denticity, substituent placement, and electron-withdrawing capacity of different catalytic scaffolding (Figure 5). The correlation between elemental composition and the size of the $\sigma$-hole was observed for both homoatomic $I_2$ and heteroatomic CAT4. Notably, the heteroatomic CAT4 displayed a larger $V_{max}$ compared to the former, attributed to a more pronounced polarisation effect within the catalytic scaffolding. The polarisation effect was further investigated in CAT3, CAT5 and CAT6, where the electron-withdrawing capacity of the scaffolding was varied. In the case of replacing the imidazolium moiety with the more electron-withdrawing benzimidazolium group (CAT3 to CAT5) $V_{max}$ for the $\sigma$-hole increased slightly from 0.267 a.u. to 0.271 a.u. However, the opposite effect was observed upon the incorporation of a trifluoromethyl group ortho to the benzimidazolium moieties as seen in CAT6, resulting in a reduced $V_{max}$ of 0.263 a.u. Consequently, CAT7 and CAT8 were computationally suggested, in order to explore the impact of the placement of the trifluoromethyl group within the catalytic scaffolding, resulting in an overall increase in $V_{max}$ (Figure 5 and Figure S11-S16).

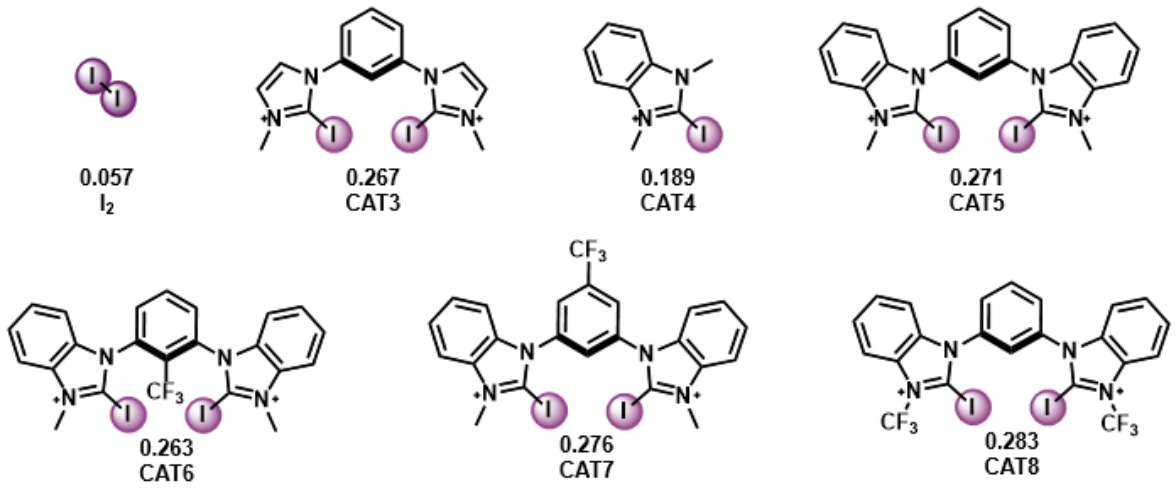


Figure 5: MEP on the 0.001 a.u. electron density isosurface and maxima ($V_{max}$) values in a.u. for the catalysts under study ($I_2$ and CAT3-8).

Additionally, the activation energy for the C-C coupling step (TS1) in the Michael addition of indole to *trans*-crotonophenone was computed and subsequently compared across the range of previously mentioned XB-based catalysts. First, we investigate the impact of the effect of the XB donor and substituent within the O activation mode, as suggested in the literature.[42] As illustrated in Figure 6, the O-activation mode involves a stabilisation interaction between the XB-donor and the carbonyl oxygen of the *trans*-crotonophenone substrate. This interaction is further characterised by the $\rho_{BCP}$, and CT process occurring from oxygen to the XB-donor atom (X1/X2) within both, the bidentate and monodentate systems.

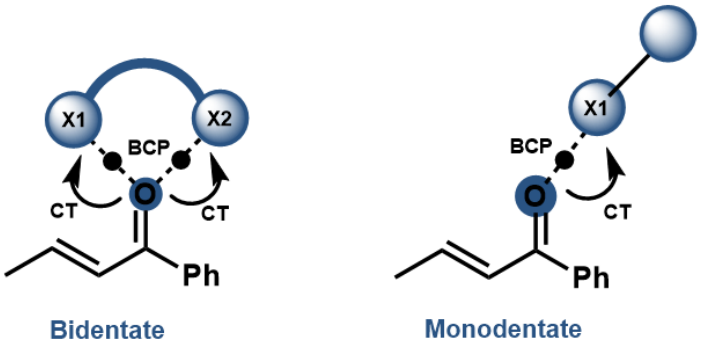


Figure 6: The *trans*-crotonophenone substrate activated by XB-based catalysts through O-activation.

In general, the trend discussed for the MEP analysis translated into the energy barriers calculated for TS1 of the Michael addition of indole to *trans*-crotonophenone (Figure 7). CAT1-3 demonstrates the XB-donor effect, emphasising that the activation energy of the reaction is in an inverse relationship with the polarisation of the XB-donor. The energy barriers calculated for the reaction under the catalysis of CAT1, CAT2, CAT4, CAT6, and $I_2$ were observed to be higher than the un-catalysed reaction, suggesting that the XB-interaction within the O-activated TS1 of the Michael addition is relatively weak and ineffective, contradictory to experimental findings reported in literature.[42] Similar to the unusually low $\sigma$-hole observed for CAT6 (as shown in Figure 5), the activation energy for CAT6 followed a

similar trend, exhibiting the highest activation energy amongst all the iodine-based catalysts (CAT3-8).

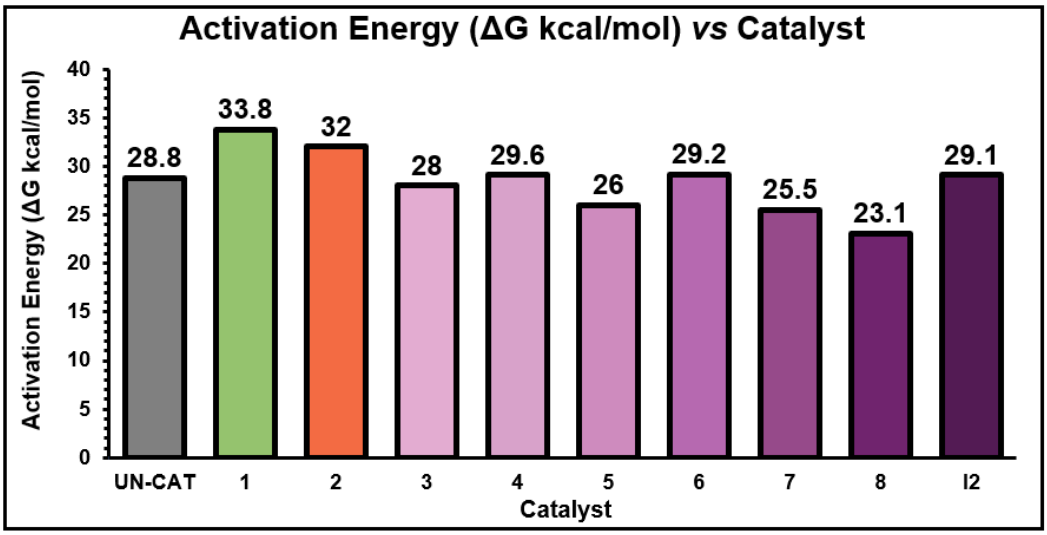


Figure 7: Activation barriers for the O-activated TS1 of the Michael addition of indole to *trans*-crotonophenone under the catalysis of a variety of XB-based organocatalysts.

A recent proposal by Robidas *et al*[43] has introduced a direct $\pi$-type activation mode for stabilising unsaturated carbonyl substrates. In the context of iodine-based XB catalysts ($I_2$, CAT3, CAT4, CAT6, and CAT7, as shown in Figure 8), this $\pi$-type activation mode has been compared to the established O-activation mode. Unlike the O-activation mode depicted in Figure 6, the $\pi$-type activation mode demonstrates varying binding behaviours in both, bidentate and monodentate systems. In the former, the XB-based catalyst activates the *trans*-crotonophenone substrate at two distinct sites simultaneously: carbonyl oxygen and the $\alpha$-carbon. In contrast, in monodentate systems, the activation exclusively occurs at the $\alpha$-carbon, as emphasised by the $\rho_{BCP}$ and CT direction illustrated in Figure 8.

As shown in Figure 9 most of the iodine-based catalysts, with the exception of CAT4, exhibit a thermodynamic preference for the $\pi$-type activation mode in the context of TS1 of the Michael addition reaction.

Although the trend of activation energy remains consistent for both the $\pi$-type and O-activation modes, the $\pi$-type activation mode shows energetic data that aligns more closely

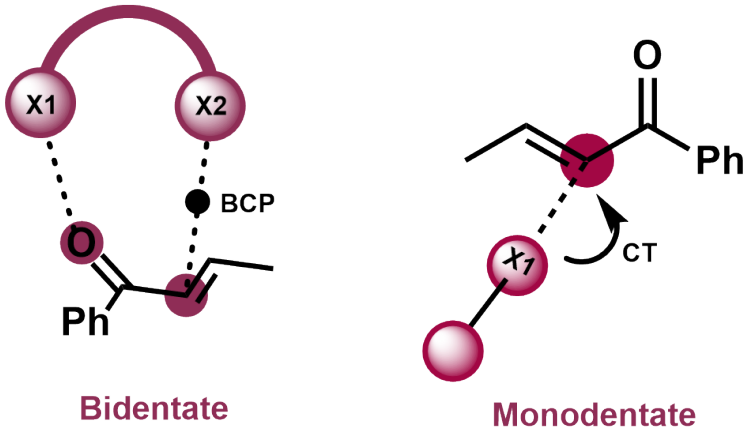


Figure 8: The *trans*-crotonophenone substrate activated by XB-based catalysts through $\pi$-type activation.

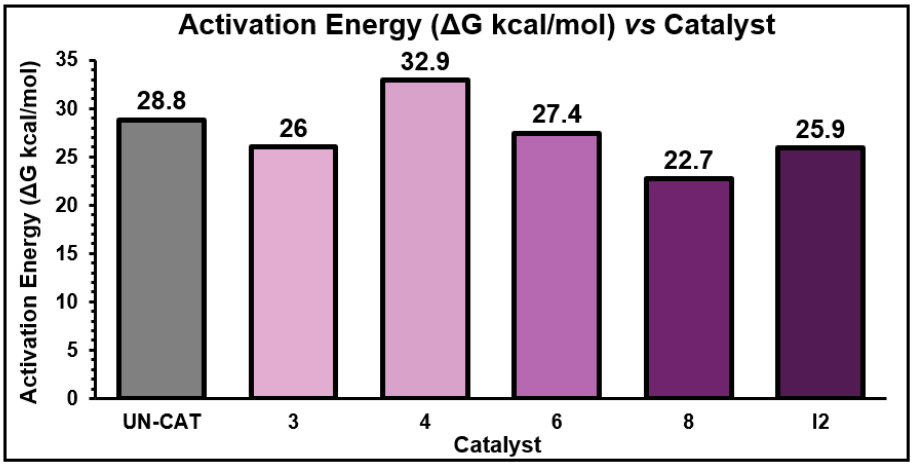


Figure 9: Activation barriers for the $\pi$-type activated TS1 of the Michael addition of indole to *trans*-crotonophenone under the catalysis of a variety of XB-based organocatalysts.

with experimental observations. Notably, when considering the O-activation mode within the CAT6 and $I_2$ catalysed TS1, the calculated activation energy suggests that the catalyst has a higher activation energy than the un-catalysed system, implying that both catalysts are not effective (Figure 7). In contrast, the energetic data for the $\pi$-type activation mode indicate much lower activation energy for CAT6 and $I_2$ catalysed TS1 (Figure 9), suggesting that both catalysts perform better than the un-catalysed reaction, in total agreement with the literature.[42] Relative to the O-activation mode, the energy barriers linked with the $\pi$-type activation mode offer theoretical predictions that align more closely with experimental

observations. This is evident in the depiction of the robust catalytic activity exhibited by $I_2$, as supported by experimental results.[44]

In summary of the analysis of the two activation modes, a structural comparison was conducted. The specific focus was on the energy required for the rotation of the dihedral angle $\alpha$ within the bidentate catalytic framework (refer to supporting information, Figure S17 and Table S12). This comparison involved extracting the catalyst's structure from the optimised TS1 of the Michael addition reaction and subsequently comparing it structurally and energetically to the monomeric catalyst structure. The results, as presented in Table 3, indicates that a positive deformation energy suggests the optimised monomeric catalyst is more stable relative to the structure of the catalyst within TS1. In particular, our findings consistently revealed relatively lower deformation energies in the $\pi$-type activated systems, indicating a less energetically demanding conformational change from the isolated to the $\pi$-type activated substrate-bound state in contrast to the O-activation mode. Interestingly, CAT6 exhibited the highest deformation energy in both the O-activated and $\pi$-type activated systems, therefore explaining the unusually high activation energy displayed by CAT6 relative to other iodine-based organocatalysts, as depicted in Figures 7 and 9.

Table 3: Deformation energy (kcal/mol) for the O- and $\pi$-type activated bidentate catalytic systems transitioning from the monomeric to substrate-bound TS1 state; obtained by extracting the energetic difference between the isolated geometry of the optimised monomeric and substrate-bound catalyst.

| **Deformation Energy (kcal/mol)** | **CAT3** | **CAT6** | **CAT8** |
|---|---|---|---|
| $\pi$-type activated TS1 | -0.07 | 1.91 | 1.06 |
| O-activated TS1 | 2.58 | 8.94 | 3.69 |

## Mechanistic analysis

The $\pi$-type and O-activated hetero- and homo-atomic catalytic systems were thoroughly assessed and compared from a mechanistic perspective. The analysis focused on understanding the underlying mechanisms of these two activation modes and their respective impact on the catalytic processes. The O- and $\pi$-type activation modes of the heteroatomic

catalysts (CAT3, CAT4, CAT6, and CAT8) exhibited different substrate activation modes but consistently shared the same anticipated[53] mechanism for TS1 (Figure 10). Notably, the $\pi$-type activated TS1 was found to be more energetically stable in all the bidentate catalytic systems, while the monodentate CAT4 showed a preference for the O-activation mode. The likely reason for this observation lies in the ability of the bidentate catalysts to simultaneously activate both sites of the *trans*-crotonophenone substrate, the carbonyl oxygen and the $\alpha$-carbon. In contrast, the monodentate CAT4 lacks this feature and is limited to interactions solely with either the carbonyl oxygen in the O-activation mode or the $\alpha$-carbon in the $\pi$-type activation mode.

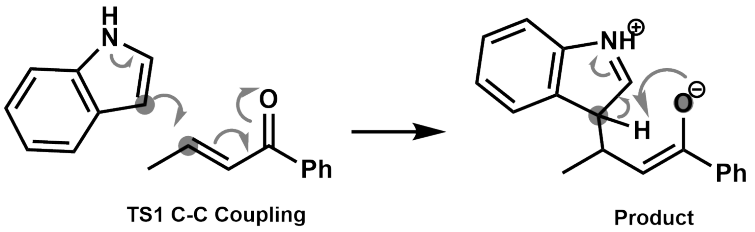


Figure 10: Mechanism of the O- and $\pi$-type activated TS1 of the Michael addition of indole to *trans*-crotonophenone under the catalysis of a series of heteroatomic XB-based scaffolds.

In contrast, the addition of indole to *trans*-crotonophenone under the catalysis of the homoatomic $I_2$ catalyst revealed evidence of different mechanisms (Figure 11), resulting in distinct free energy profiles. Under the catalytic influence of $I_2$, the $\pi$-type activated pathway demonstrated lower energy barriers for both the C-C coupling (TS1) and proton transfer (TS2) steps compared to the O-activated pathway. The calculated activation energy for O-activated TS1 was 29.1 kcal/mol, whereas the $\pi$-type activated barrier was reduced to 25.9 kcal/mol, resulting in an overall $\Delta\Delta G$ of 3.2 kcal/mol. Similarly, O-activated TS2 had an energy of 22.8 kcal/mol, while the $\pi$-type activated TS2 energy was notably lower at 12.4 kcal/mol, resulting in a significant $\Delta\Delta G$ difference of 10.4 kcal/mol (refer to supplementary information, Figure S18 and Table S13, for a comprehensive free energy profile).

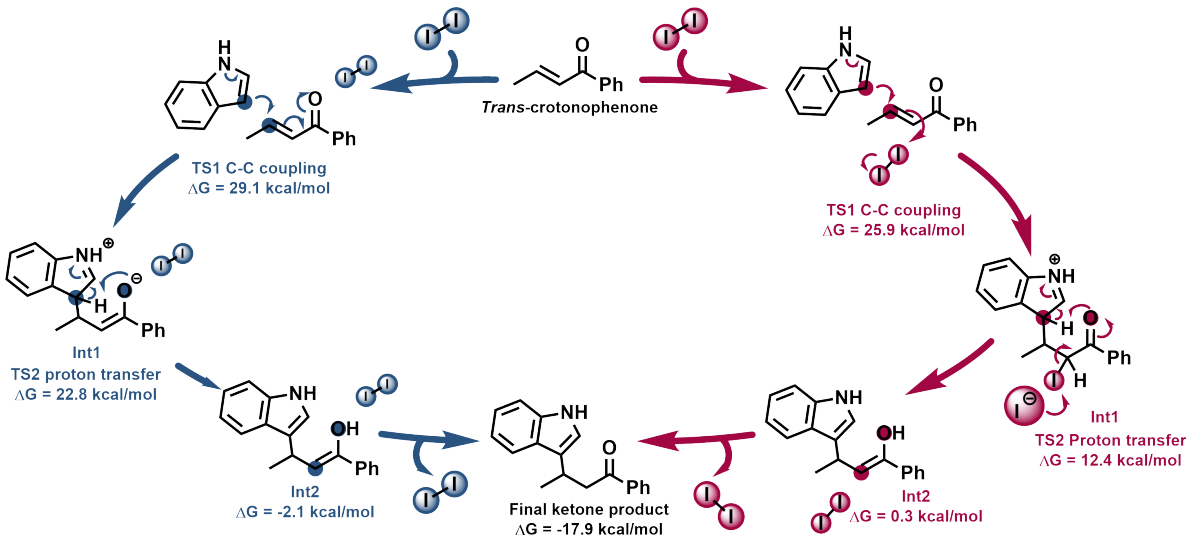


Figure 11: Mechanism of the O- (blue) and $\pi$-type (red) activated Michael addition reaction of indole to *trans*-crotonophenone under the catalysis of $I_2$ including the corresponding $\Delta$G (kcal/mol).

### Nature of the $\pi$-type activated Michael addition via $I_2$

The use of $I_2$ as a catalyst to enhance a broad range of organic reactions has been firmly established and acknowledged in the literature.[54,55] Despite its structural simplicity, iodine offers several notable advantages, including cost efficiency and environmental sustainability. However, the precise mechanism underlying its highly robust catalytic activity has remained a subject of debate, leading to active discussions and various explanations proposed over the past decades.[56] Considering this, the unexpectedly efficient mechanism discovered for the $\pi$-type activated Michael addition catalysed by $I_2$ has been meticulously characterised and elaborated. This analysis aimed to gain mechanistic insights into the complex nature of the interaction between $I_2$ and the $\alpha$-carbon of the $\pi$-type activated *trans*-crotonophenone substrate. The investigation encompasses an extensive exploration of various structural attributes, including bond lengths, hybridisation angles, and characterisation of the interaction using QTAIM methods and descriptors, including $\rho_{BCP}$, Laplacian ($\nabla^2\rho(r)$), and H value. To ensure a comparative analysis, geometrically optimised control compounds were used, as demonstrated in Figure 12.

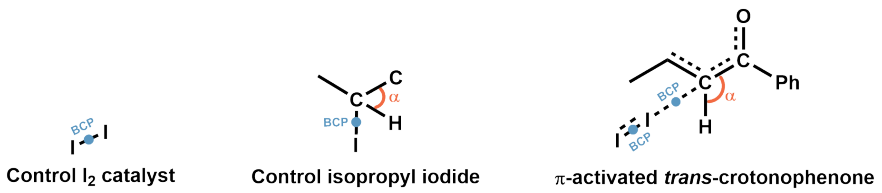


Figure 12: Electronic features and bond length measured at the $\rho_{BCP}$ (red) as well as the angle of hybridisation $\alpha$ (blue) of the $\pi$-type activated *trans*-crotonophenone under the catalysis of $I_2$.

The investigation revealed an intriguing transitional nature in the interaction of the $I_2$ catalyst with the $\pi$-type activated *trans*-crotonophenone substrate. This interaction displayed a dynamic interplay between non-covalent and weakly covalent interactions throughout the entire mechanistic pathway of the Michael addition reaction relative to the control molecules. The most prominent change in the nature of the substrate-bound $I_2$ catalyst was observed within Int1, as evidenced by variations in the bond length, $\rho_{BCP}$, and the H value (Table 4). These findings indicate a change from covalent to non-covalent characteristics in the $I_2$ catalyst while activating the *trans*-crotonophenone substrate. Furthermore, in addition to the aforementioned data that elucidate the nature of the $I_2$ catalyst, the same investigation was conducted to examine the nature of the interaction between $I_2$ and the $\alpha$-carbon of the *trans*-crotonophenone substrate, comparing it to the geometrically optimised C-I bond in the isopropyl iodide control molecule. Similar to the $I_2$ catalyst, the most notable and significant transition in nature was observed within Int1 of the reaction pathway (Table 5). The transition was noted to shift from a non-covalent interaction to a weakly covalent bond, supported by various characteristics, including the short bond length, negative $\nabla^2\rho(r)$ and H value, as well as the angle of hybridisation, which closely resembled that of a $sp^3$ hybridised carbon.

The phenomenon of $I_2$ forming covalent bonds with unsaturated hydrocarbon compounds is a well-established concept and has been extensively observed in the electrophilic iodination of organic compounds using $I_2$ in appropriate solvents.[57,58] In the context of iodofluorination of $\alpha$-$\beta$-unsaturated esters, it has been reported that the iodonium cation forms a covalent

Table 4: Structural and electronic features of the $I_2$ catalyst bound to the *trans*-crotonophenone substrate in the full mechanistic pathway of the Michael addition reaction, compared to the control isolated $I_2$ catalyst.

| **I-I** | **TS1** | **Int1** | **TS2** | **Int2** | **Control** |
|---|---|---|---|---|---|
| Bond length (Å) | 3.032 | 3.69 | 3.51 | 2.74 | 2.69 |
| $\rho_{BCP}$ (a.u.) | 0.038 | 0.011 | 0.016 | 0.066 | 0.072 |
| $\nabla^2\rho_{BCP}$ (a.u.) | 0.048 | 0.027 | 0.035 | 0.014 | 0.0033 |
| H value | -0.0066 | 0.00080 | -0.00029 | -0.016 | - |

bond at the $\alpha$-carbon position,[59] in a similar fashion to the observations reported herein for the $\pi$-type activated TS1 of the $I_2$ catalysed Michael addition reaction. Compared to other diatomic atoms in the halogen series, $I_2$ exhibits the lowest thermodynamic barrier for transitioning from $I_2$ to $I^-$, in line with its relatively low reduction potential.[60] Therefore, the observed conversion of $I_2$ to $I^-$ throughout the $\pi$-type activated Michael addition of indole to *trans*-crotonophenone, as documented in this study, can be considered within the expected behaviour of $I_2$ upon interaction with the $\alpha$-$\beta$-unsaturated hydrocarbon molecules. The transitional nature of the interaction between $I_2$ and the $\alpha$-carbon of the *trans*-crotonophenone serves as a driving force for the $\pi$-type activated Michael addition reaction, playing a crucial role in facilitating the transformation.

Table 5: Structural and QTAIM analysis of the $I_2$ catalyst bound to the *trans*-crotonophenone substrate in the full mechanistic pathway of the Michael addition reaction, compared to the control isopropyl iodide molecule.

| **C-I** | **TS1** | **Int1** | **TS2** | **Int2** | **Control** |
|---|---|---|---|---|---|
| Bond length (Å) | 2.42 | 2.20 | 2.22 | 3.022 | 2.20 |
| $\rho_{BCP}$ (a.u.) | 0.07 | 0.11 | 0.10 | 0.02 | 0.11 |
| $\nabla^2\rho_{BCP}$ (a.u.) | 0.044 | -0.026 | -0.0088 | 0.045 | -0.063 |
| H value | -0.014 | -0.0460 | -0.037 | -0.0002 | - |
| $\alpha$ (°) | 115.16 | 110.68 | 112.27 | 118.48 | 110.54 |

Furthermore, the physical origin of $\pi$-type activated TS1 in the Michael addition reaction was examined using LMO-EDA. The main objective was to gain clarity and justification for the evident preference for the $\pi$-type activation mode in the $I_2$ catalysed reaction. First, the energetic components that contribute to the overall interaction energy between the indole

and $I_2$ activated *trans*-crotonophenone were compared in the O- and $\pi$-type activation modes (Figure 13).

The interaction was more stable in the $\pi$-type activation TS1, as indicated by the total interaction energy, primarily driven by the decrease in Pauli repulsion forces between the indole and *trans*-crotonophenone (Figure 13). Following, the energetic components accounting for the overall stabilisation interaction between the O- and $\pi$-type activated *trans*-crotonophenone and $I_2$ catalyst were evaluated. Despite the $\pi$-type activated interaction displaying a significantly larger repulsive energy component, the interaction exhibited higher stability than the O-activation mode. The remaining energetic components, particularly the electrostatic, exchange and polarisation components, were found to be more stable within the $\pi$-type activated interaction, contributing to the overall stability of the stabilisation interaction. Additionally, the relatively large repulsive energy component in the $\pi$-type activated interaction can be attributed to the slightly covalent nature of the interaction between the $\pi$-type activated *trans*-crotonophenone and $I_2$ catalyst. In contrast to the other monodentate catalyst under investigation, CAT4, the LMO-EDA analysis of the stabilisation interaction between CAT4 and the *trans*-crotonophenone substrate demonstrated that its preference for the O-activation mode is solely governed by the electrostatic and repulsive energy components (Figure 13).

### Characterisation of the NCIs

The NCIs between the XB donor atom (X) and the oxygen atom (O) of *trans*-crotonophenone substrate were characterised to obtain a detailed examination of the nature and relative strength of the interactions involved in the O-activated (see Figure 6) TS1 of the Michael addition reaction under the catalysis of various XB-based scaffolds.

The XB interaction between X and O, as presented in Tables 6 and 7, was in agreement with both the QTAIM and NBO methods and provided further validation for the previously discussed concepts related to the XB-donor and substituent effects. In relation to CAT6, it

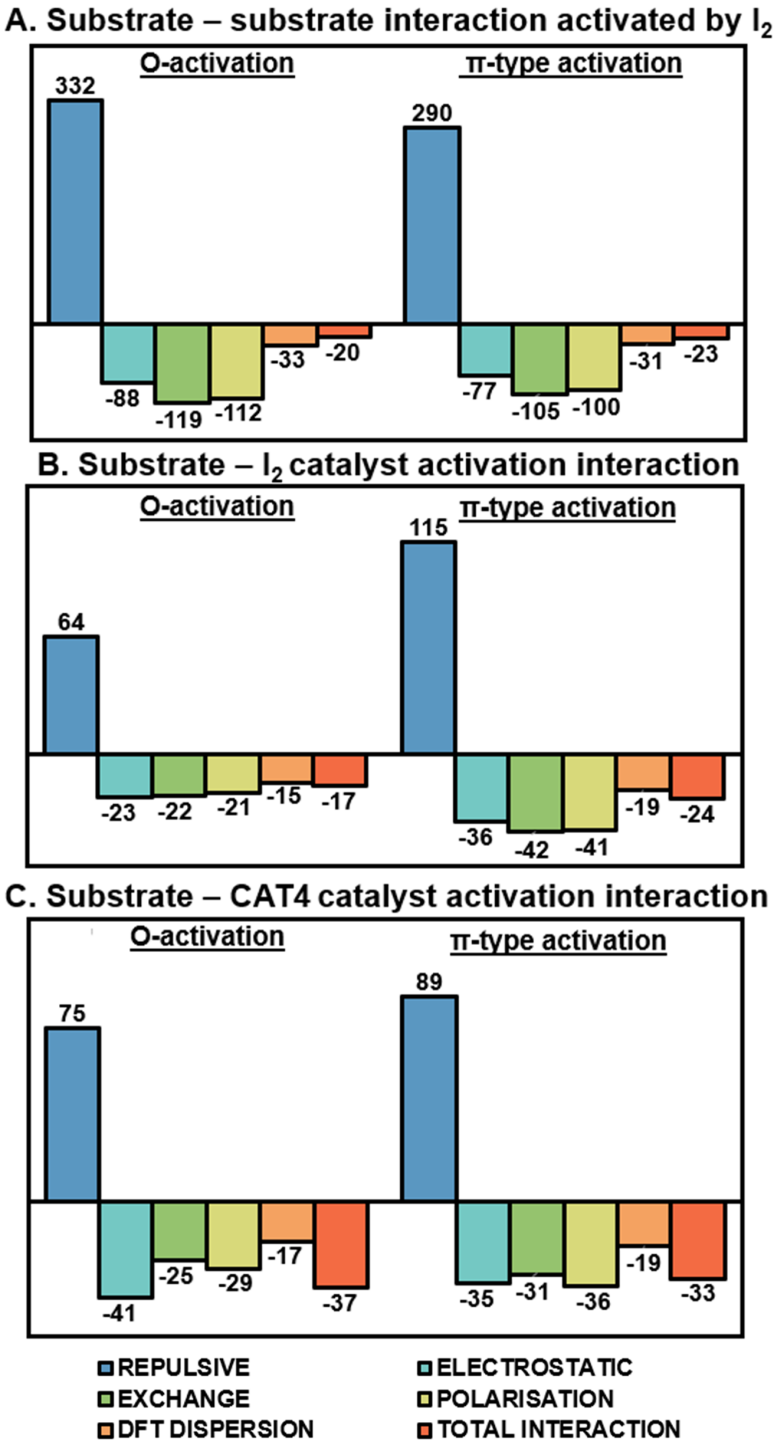


Figure 13: LMO-EDA energy partition terms for the interaction between indole and the O- and $\pi$-type activated *trans*-crotonophenone under the $I_2$ catalysed TS1 of the Michael addition reaction (A). LMO-EDA energy partition terms for the stabilisation interaction between indole and the O- and $\pi$-type activated *trans*-crotonophenone under the $I_2$ and CAT4 catalysed TS1 of the Michael addition reaction (B and C).

Table 6: $\rho_{BCP}$ (a.u.) for the O···X interaction within the O-activated TS1 of the Michael addition of indole to *trans*-crotonophenone under the catalysis of a series of XB-based catalysts

| $\rho_{BCP}$ **(a.u.)** | **CAT1** | **CAT2** | **CAT3** | **CAT4** | **CAT5** | **CAT6** | **CAT7** | **CAT8** |
|---|---|---|---|---|---|---|---|---|
| O···X1 | 0.018 | 0.021 | 0.024 | 0.038 | 0.026 | 0.027 | 0.027 | 0.030 |
| O···X2 | 0.016 | 0.022 | 0.022 | - | 0.022 | 0.026 | 0.025 | 0.028 |
| **Total** | **0.034** | **0.043** | **0.047** | **0.038** | **0.048** | **0.052** | **0.052** | **0.057** |

should be noted that the $\rho_{BCP}$ values obtained and E(2) outcome do not correspond with the relatively high calculated activation energy barrier observed in the CAT6-catalysed TS1 of the Michael addition reaction (as depicted in Figures 7 and 9). Nevertheless, the trend derived for the XB-interactions, quantified using methods namely QTAIM and NBO, aligns with experimental findings,[42] where CAT1 < CAT2 < CAT3 < CAT5 < CAT6.

Table 7: NBO E(2) (kcal/mol) for the O···X interaction within the O-activated TS1 of the Michael addition of indole to *trans*-crotonophenone under the catalysis of a series of XB-based catalysts

| **O···X (1kcal/mol)** | **CAT1** | **CAT2** | **CAT3** | **CAT5** | **CAT6** | **CAT7** | **CAT8** |
|---|---|---|---|---|---|---|---|
| LP 1 (O) ->BD*(C-X1) | 1.52 | 3.61 | 6.96 | 6.94 | 7.13 | 8.09 | 8.21 |
| LP 1 (O) ->BD*(C-X2) | 0.57 | 1.68 | 7.79 | 8.03 | 8.51 | 6.71 | 9.23 |
| LP 2 (O) ->BD*(C-X1) | 0.39 | 1.17 | 0.97 | 2.58 | 3.49 | 1.41 | 2.95 |
| LP 2 (O) ->BD*(C-X2) | 0.69 | 1.16 | 2.09 | 1.92 | 1.32 | 5.09 | 3.75 |
| LP 3 (O) ->BD*(C-X1) | 1.79 | 0.060 | 4.45 | 5.42 | 4.75 | 3.43 | 7.54 |
| LP 3 (O) ->BD*(C-X2) | - | 3.46 | 4.46 | 2.9 | 4.13 | 3.65 | 2.16 |
| **Total** | **4.96** | **11.14** | **26.72** | **27.79** | **29.33** | **28.38** | **33.84** |

Furthermore, the interaction between X and O atoms in the activated O- and $\pi$-type activated systems was quantified and compared. The results revealed that in the bidentate catalytic systems CAT3, CAT6, and CAT7, the E(2) and $\rho_{BCP}$ between the O and the X was enhanced in the $\pi$-type activation mode (Figure 14 and Figure 15). For a complete and detailed version of Figure 14, please refer to the supplementary information, Table S14. In contrast, for $I_2$, E (2) and $\rho_{BCP}$ exhibited an overall increase in the $\pi$-type activated system, resembling a slight covalent nature, while the opposite was observed for CAT4, which had an increase in CT and $\rho_{BCP}$ within the O-activated mode (Figure 14 and Figure 15). The bidentate XB-based organocatalysts exhibit a clear preference for the $\pi$-type activation mode

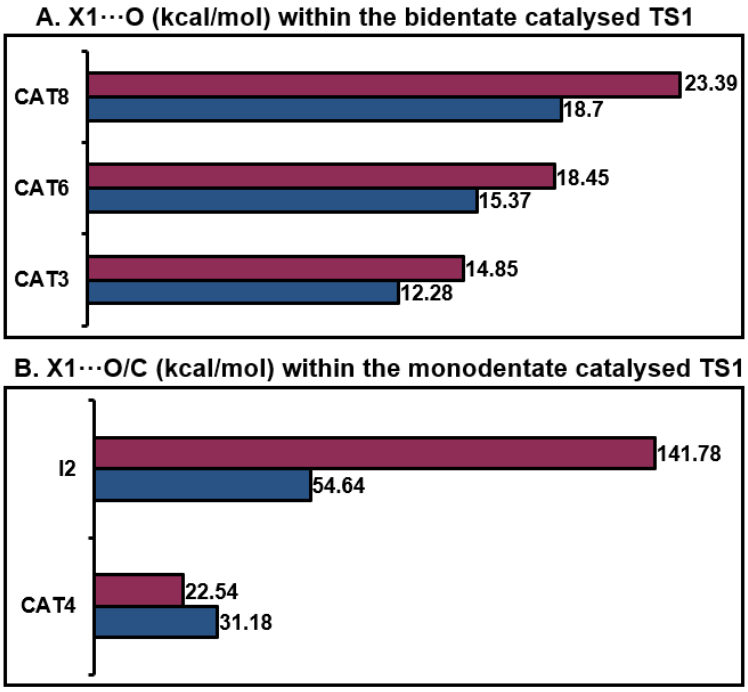


Figure 14: NBO E(2) (kcal/mol) for the O···X interaction within the bidentate catalytic systems (A). and the O/C···X interactions within bidentate catalytic systems (B). in the O- (blue) and $\pi$-type (red) activated TS1 of the Michael addition of indole to *trans*-crotonophenone

due to their ability to simultaneously activate both active sites of the *trans*-crotonophenone substrate, i.e., the carbonyl oxygen and the $\alpha$-carbon. On the other hand, the preference trends observed for the monodentate catalysts can be attributed primarily to the nature of the binding interaction. Monodentate $I_2$ and CAT4 can only interact with the substrate through carbonyl oxygen or the $\alpha$-carbon. The stronger non-covalent interaction between CAT4 and the carbonyl oxygen (as reflected in Figure 14 and Figure 15) relative to the interaction with the $\alpha$-carbon results in the energetic preference for the O-activation mode. Conversely, the $I_2$ catalyst shows a preference for the $\pi$-type activation mode because of the relatively stronger dual non-covalent to slightly covalent nature of the interaction with the $\alpha$-carbon, relative to the primarily non-covalent interaction with the O atom, as seen in the O-activation mode (see supporting information Table S14 and S15).

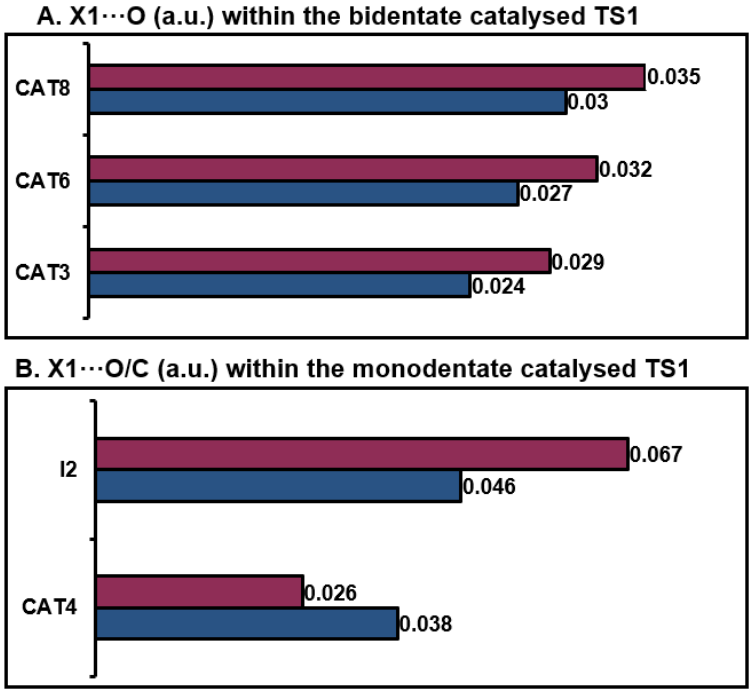


Figure 15: $\rho_{BCP}$ (a.u.) for the O···X interaction within the bidentate catalytic systems (A). and the O/C···X interactions within bidentate catalytic systems (B). in the O- (blue) and $\pi$-type (red) activated TS1 of the Michael addition of indole to *trans*-crotonophenone

# Conclusion

Up to the present date, DFT methodology was employed to explore the explicit pathway and substrate-catalyst binding mode of the Ritter-type solvolysis reaction catalysed by XB-based CAT3 and CAT9. The investigation revealed that both catalytic systems strongly favour Pathway 1, suggesting that the XB-donor engages in NCIs with the R-X leaving group, initiating a heterolytic bond cleavage process, followed by an acetonitrile N-terminal attack. Notably, CAT3 and CAT9 exhibit distinct substrate binding modes: CAT3 adopts a bidentate binding mode, whereas CAT9 demonstrates a clear energetic preference for the monodentate mode, facilitated by secondary NCIs between the catalyst and the substrate. Despite these different binding modes, a direct comparison of the catalytic efficiency of CAT3 and CAT9 in the halide abstraction reaction reveals remarkably similar activities, a conclusion supported by both experimental sources[41,52] and theoretical data.

The exploration of the Michael addition of indole to *trans*-crotonophenone, catalysed

by a diverse range of XB-based catalysts, has provided profound insights into the catalyst-substrate interaction. Electronic properties of the XB-donor and the catalytic scaffold influence the size of the hole $\sigma$, while steric effects between the XB-donor atom and catalytic scaffolding also play a critical role. CAT6, CAT7, and CAT8 highlighted the importance of XB-donor atom positioning within the catalytic scaffolding, specifically in terms of how it affects $\sigma$-hole size and catalytic deformation energy. The recently proposed $\pi$-type activation mode[43] was compared with the more discussed O-activation mode. Remarkably, the theoretical results of the $\pi$-type activation mode align more closely with the experimental data and are thermodynamically preferred by the bidentate scaffolds and $I_2$. This mode has unveiled an alternative mechanistic pathway characterised by a dual non-covalent and slightly covalent nature for $I_2$ catalysed Michael addition of indole to *trans*-crotonophenone, providing insights into the reaction mechanism of this robust catalyst. Heteroatomic bidentate scaffolds preferred the $\pi$-type activation mode due to the ability of the scaffolds to simultaneously bind to both active sites of *trans*-crotonophenone; the carbonyl oxygen and $\alpha$-carbon. For the homoatomic $I_2$, its $\pi$-type activation preference arose from its unique and relatively strong dual non-covalent and slightly covalent interaction with the substrate's $\alpha$-carbon. Understanding these activation modes and their interactions is crucial for the design of efficient XB-based organocatalysts for a broad spectrum of chemical transformations. This research provides insight into the intricate interplay of electronic and steric factors in XB-based catalysis, thereby enhancing our understanding of catalyst-substrate interactions. Such insights hold the potential to advance the application of XB-based catalysts in asymmetric organocatalysis.

# Acknowledgement

This publication has emanated from research supported by the Irish Research Council (GOIPG/2021/300). For the purpose of Open Access, the author has applied a CC BY

public copyright licence to any Author Accepted Manuscript version arising from this submission. The authors acknowledge the assistance given by Research IT and the use of the Computational Shared Facility at The University of Manchester. The authors thank the Irish Centre for High-End Computing (ICHEC) for their continued computational support.

## Supporting Information Available

All the data used in the analysis of the results can be found in the Supporting Information: https://doi.org/10.5281/zenodo.8275982

## References

(1) Edwards, J. O.; Pearson, R. G. bThe Factors Determining Nucleophilic Reactivities/b. *Journal of the American Chemical Society* **1962**, *84*, 16–24.

(2) Lorpaiboon, W.; Bovonsombat, P. Halogen bond-induced electrophilic aromatic halogenations. *Organic &amp Biomolecular Chemistry* **2021**, *19*, 7518–7534.

(3) Beale, T. M.; Chudzinski, M. G.; Sarwar, M. G.; Taylor, M. S. Halogen bonding in solution: thermodynamics and applications. *Chem. Soc. Rev.* **2013**, *42*, 1667–1680.

(4) Cavallo, G.; Metrangolo, P.; Milani, R.; Pilati, T.; Priimagi, A.; Resnati, G.; Terraneo, G. The Halogen Bond. *Chemical Reviews* **2016**, *116*, 2478–2601.

(5) Metrangolo, P.; Pilati, T.; Resnati, G. Halogen bonding and other noncovalent interactions involving halogens: a terminology issue. *CrystEngComm* **2006**, *8*, 946.

(6) Costa, P. J.; Nunes, R.; Vila-Viçosa, D. Halogen bonding in halocarbon-protein complexes and computational tools for rational drug design. *Expert Opinion on Drug Discovery* **2019**, *14*, 805–820.

(7) Montaña, Á. M. The and Holes. The Halogen and Tetrel Bondings: Their Nature, Importance and Chemical, Biological and Medicinal Implications. *ChemistrySelect* **2017**, *2*, 9094–9112.

(8) Pelletier, P. Mémoire sur un nouvel alcali végétal (la strychnine) trouvé dans la fève de Saint-Ignace, la noix vomique, etc. *Ann. Chim. Phys.* **1819**, *10*, 142–177.

(9) Brinck, T.; Murray, J. S.; Politzer, P. Molecular surface electrostatic potentials and local ionization energies of Group V-VII hydrides and their anions: Relationships for aqueous and gas-phase acidities. *International Journal of Quantum Chemistry* **1993**, *48*, 73–88.

(10) Murray, J. S.; Paulsen, K.; Politzer, P. Molecular surface electrostatic potentials in the analysis of non-hydrogen-bonding noncovalent interactions. *Proceedings / Indian Academy of Sciences* **1994**, *106*, 267–275.

(11) Auffinger, P.; Hays, F. A.; Westhof, E.; Ho, P. S. Halogen bonds in biological molecules. *Proceedings of the National Academy of Sciences* **2004**, *101*, 16789–16794.

(12) Awwadi, F. F.; Willett, R. D.; Peterson, K. A.; Twamley, B. The Nature of Halogen···Halogen Synthons: Crystallographic and Theoretical Studies. *Chemistry - A European Journal* **2006**, *12*, 8952–8960.

(13) Murray, J. S.; Lane, P.; Politzer, P. Expansion of the -hole concept. *Journal of Molecular Modeling* **2008**, *15*, 723–729.

(14) Politzer, P.; Murray, J. S.; Clark, T. Halogen bonding and other -hole interactions: a perspective. *Physical Chemistry Chemical Physics* **2013**, *15*, 11178.

(15) Desiraju, G. R.; Ho, P. S.; Kloo, L.; Legon, A. C.; Marquardt, R.; Metrangolo, P.; Politzer, P.; Resnati, G.; Rissanen, K. Definition of the halogen bond (IUPAC Recommendations 2013). *Pure and Applied Chemistry* **2013**, *85*, 1711–1713.

(16) Peluso, P.; Mamane, V. Stereoselective Processes Based on sigma;-Hole Interactions. *Molecules* **2022**, *27*.

(17) Kolář, M. H.; Hobza, P. Computer Modeling of Halogen Bonds and Other -Hole Interactions. *Chemical Reviews* **2016**, *116*, 5155–5187.

(18) Tarannam, N.; Shukla, R.; Kozuch, S. Yet another perspective on hole interactions. *Physical Chemistry Chemical Physics* **2021**, *23*, 19948–19963.

(19) Thirman, J.; Engelage, E.; Huber, S. M.; Head-Gordon, M. Characterizing the interplay of Pauli repulsion, electrostatics, dispersion and charge transfer in halogen bonding with energy decomposition analysis. *Physical Chemistry Chemical Physics* **2018**, *20*, 905–915.

(20) Mallada, B.; Gallardo, A.; Lamanec, M.; de la Torre, B.; Špirko, V.; Hobza, P.; Jelinek, P. Real-space imaging of anisotropic charge of -hole by means of Kelvin probe force microscopy. *Science* **2021**, *374*, 863–867.

(21) Jentzsch, A. V.; Matile, S. *Topics in Current Chemistry*; Springer International Publishing, 2014; pp 205–239.

(22) Pizzi, A.; Pigliacelli, C.; Bergamaschi, G.; Gori, A.; Metrangolo, P. Biomimetic engineering of the molecular recognition and self-assembly of peptides and proteins via halogenation. *Coordination Chemistry Reviews* **2020**, *411*, 213242.

(23) Žabka, M.; Šebesta, R. Experimental and Theoretical Studies in Hydrogen-Bonding Organocatalysis. *Molecules* **2015**, *20*, 15500–15524.

(24) Malerich, J. P.; Hagihara, K.; Rawal, V. H. Chiral Squaramide Derivatives are Excellent Hydrogen Bond Donor Catalysts. *Journal of the American Chemical Society* **2008**, *130*, 14416–14417.

(25) Connon, S. J. Organocatalysis Mediated by (Thio)urea Derivatives. *Chemistry - A European Journal* **2006**, *12*, 5418–5427.

(26) Joly, G. D.; Jacobsen, E. N. Thiourea-Catalyzed Enantioselective Hydrophosphonylation of Imines: Practical Access to Enantiomerically Enriched -Amino Phosphonic Acids. *Journal of the American Chemical Society* **2004**, *126*, 4102–4103.

(27) Inokuma, T.; Hoashi, Y.; Takemoto, Y. Thiourea-Catalyzed Asymmetric Michael Addition of Activated Methylene Compounds to , -Unsaturated Imides: Dual Activation of Imide by Intra- and Intermolecular Hydrogen Bonding. *Journal of the American Chemical Society* **2006**, *128*, 9413–9419.

(28) Vakulya, B.; Varga, S.; Csámpai, A.; Soós, T. Highly Enantioselective Conjugate Addition of Nitromethane to Chalcones Using Bifunctional Cinchona Organocatalysts. *Organic Letters* **2005**, *7*, 1967–1969.

(29) Taylor, M. S.; Jacobsen, E. N. Asymmetrische Katalyse durch chirale Wasserstoffbrückendonoren. *Angewandte Chemie* **2006**, *118*, 1550–1573.

(30) Hoashi, Y.; Okino, T.; Takemoto, Y. Enantioselective Michael Addition to , -Unsaturated Imides Catalyzed by a Bifunctional Organocatalyst. *Angewandte Chemie International Edition* **2005**, *44*, 4032–4035.

(31) Yamaoka, Y.; Miyabe, H.; Takemoto, Y. Catalytic Enantioselective Petasis-Type Reaction of Quinolines Catalyzed by a Newly Designed Thiourea Catalyst. *Journal of the American Chemical Society* **2007**, *129*, 6686–6687.

(32) Takagi, K.; Murakata, H.; Hasegawa, T. Application of Thiourea/Halogen Bond Donor Cocatalysis in Metal-Free Cationic Polymerization of Isobutyl Vinyl Ether and Styrene Derivatives. *Macromolecules* **2022**, *55*, 5756–5765.

(33) Metrangolo, P.; Neukirch, H.; Pilati, T.; Resnati, G. Halogen Bonding Based Recognition Processes: A World Parallel to Hydrogen Bonding. *Accounts of Chemical Research* **2005**, *38*, 386–395.

(34) Wolters, L. P.; Bickelhaupt, F. M. Halogen Bonding versus Hydrogen Bonding: A Molecular Orbital Perspective. *ChemistryOpen* **2012**, *1*, 96–105.

(35) Politzer, P.; Murray, J. S.; Clark, T. Halogen bonding: an electrostatically-driven highly directional noncovalent interaction. *Physical Chemistry Chemical Physics* **2010**, *12*, 7748.

(36) de Azevedo Santos, L.; Ramalho, T. C.; Hamlin, T. A.; Bickelhaupt, F. M. Intermolecular Covalent Interactions: Nature and Directionality. *Chemistry – A European Journal* **2023**, *29*.

(37) Metrangolo, P.; Resnati, G.; Pilati, T.; Biella, S. *Halogen Bonding*; Springer Berlin Heidelberg, pp 105–136.

(38) Keuper, A. C.; Fengler, K.; Ostler, F.; Danelzik, T.; Piekarski, D. G.; Mancheño, O. G. Fine-tuning Substrate–Catalyst Halogen–Halogen Interactions for Boosting Enantioselectivity in Halogen-Bonding Catalysis. *Angewandte Chemie International Edition* **2023**,

(39) Bolm, C.; Bruckmann, A.; Pena, M. Organocatalysis through Halogen-Bond Activation. *Synlett* **2008**, *2008*, 900–902.

(40) Peluso, P.; Mamane, V. Stereoselective Processes Based on -Hole Interactions. *Molecules* **2022**, *27*, 4625.

(41) Walter, S. M.; Kniep, F.; Herdtweck, E.; Huber, S. M. Halogen-Bond-Induced Activation of a Carbon-Heteroatom Bond. *Angewandte Chemie International Edition* **2011**, *50*, 7187–7191.

(42) Gliese, J.-P.; Jungbauer, S. H.; Huber, S. M. A halogen-bonding-catalyzed Michael addition reaction. *Chemical Communications* **2017**, *53*, 12052–12055.

(43) Robidas, R.; Legault, C. Y. Direct -Activation vs. iO/i -Activation in Halogen-Bonding Catalysis. *Angewandte Chemie International Edition* **2023**, *62*.

(44) von der Heiden, D.; Bozkus, S.; Klussmann, M.; Breugst, M. Reaction Mechanism of Iodine-Catalyzed Michael Additions. *The Journal of Organic Chemistry* **2017**, *82*, 4037–4043.

(45) Frisch, M. J. et al. Gaussian 09, Revision A.02. 2016; Gaussian, Inc., Wallingford CT.

(46) Bader, R. F. W.; Carroll, M. T.; Cheeseman, J. R.; Chang, C. Properties of atoms in molecules: atomic volumes. *Journal of the American Chemical Society* **1987**, *109*, 7968–7979.

(47) Lu, T.; Chen, F. T. Lu, F. Chen. *Journal of Computational Chemistry* **2012**, *33*, 580–592.

(48) Keith, T. A. AIMAll. TK Gristmill Software, 2011; `http://aim.tkgristmill.com`.

(49) Reed, A. E.; Curtiss, L. A.; Weinhold, F. A. E. Reed, L. A. Curtiss, F. Weinhold. *Chemical Reviews* **1988**, *88*, 899–926.

(50) Su, P.; Li, H. P. Su, H. Li. *The Journal of Chemical Physics* **2009**, *131*, 014102.

(51) Schmidt, M. W.; Baldridge, K. K.; Boatz, J. A.; Elbert, S. T.; Gordon, M. S.; Jensen, J. H.; Koseki, S.; Matsunaga, N.; Nguyen, K. A.; Su, S.; Windus, T. L.; Dupuis, M.; Montgomery, J. A., Jr M. W. Schmidt, K. K. Baldridge, J. A. Boatz, S. T. Elbert, M. S. Gordon, J. H. Jensen, S. Koseki, N. Matsunaga, K. A. Nguyen, S. Su, T. L. Windus, M. Dupuis, J. A. Montgomery, Jr. *Journal of Computational Chemistry* **1993**, *14*, 1347–1363.

(52) Perera, M. D.; Aakeröy, C. B. Organocatalysis by a multidentate halogen-bond donor: an alternative to hydrogen-bond based catalysis. *New Journal of Chemistry* **2019**, *43*, 8311–8314.

(53) Sun, Y.; Li, Y.; Li, X.; Zeng, Y. The mechanism and impact of mono/bis(iodoimidazolium) halogen bond donor catalysts on Michael addition of indole with itrans/i-crotonophenone: DFT calculations. *Physical Chemistry Chemical Physics* **2022**, *24*, 6690–6698.

(54) Banerjee, A. K.; Vera, W.; Mora, H.; Laya, M. S.; Bedoya, L.; Cabrera, E. V. Iodine in organic synthesis. **2006**,

(55) Jereb, M.; Vražič, D.; Zupan, M. Iodine-catalyzed transformation of molecules containing oxygen functional groups. *Tetrahedron* **2011**, *67*, 1355–1387.

(56) Breugst, M.; von der Heiden, D. Mechanisms in Iodine Catalysis. *Chemistry - A European Journal* **2018**, *24*, 9187–9199.

(57) Stavber, S.; Jereb, M.; Zupan, M. Electrophilic Iodination of Organic Compounds Using Elemental Iodine or Iodides. *Synthesis* **2008**, *2008*, 1487–1513.

(58) Ajvazi, N.; Stavber, S. Electrophilic Iodination of Organic Compounds Using Elemental Iodine or Iodides: Recent Advances 2008ndash;2021: Part I. *Compounds* **2022**, *2*, 3–24.

(59) Nagura, H.; Kuribayashi, S.; Ishiguro, Y.; Inagi, S.; Fuchigami, T. Electrochemical iodofluorination of electron-deficient olefins. *Tetrahedron* **2010**, *66*, 183–186.

(60) Luján-Montelongo, J. A.; Mateus-Ruiz, J. B.; Valdez-García, R. M. Iodine and Iodide in Reductive Transformations. *European Journal of Organic Chemistry* **2023**, *26*.